Plant Soil (2026) 518:1035–1054
https://doi.org/10.1007/s11104-025-08046-6

RESEARCH ARTICLE

Experimental insights into mucilage-mediated nutrient diffusion in different soil textures

Bahareh Hosseini · Meysam Cheraghi · Daniel Sebastian Moser · Maire Holz · Valerie Pusch · Rainer Remus · Mohsen Zarebanadkouki

Received: 1 November 2024 / Accepted: 22 October 2025 / Published online: 24 November 2025

Abstract

Background and Aims Volumetric soil water content (θ_v) strongly regulates nutrient diffusion, particularly under drying conditions. This study investigates how plant-derived mucilage alters water retention and the effective diffusion coefficient (D_s) of calcium (Ca^{2+}) in soils with contrasting textures (sand, sandy loam, and loam) under varying θ_v.

Methods We amended soils with maize mucilage at contents (C_m) of 0.0, 2.5, 5.0, and 7.5 mg/g adjusted them to three θ_v levels. A ^{45}Ca tracer and phosphor imaging were used to track Ca^{2+} diffusion over time. D_s was estimated from the ^{45}Ca distribution, allowing evaluation of mucilage effects on water retention and solute transport.

Results Mucilage effects were strongly texture- and θ_v-dependent. In loam, mucilage enhanced θ_v and D_s at the same soil matric potential (ψ_{soil}); for example, at a θ_v of 0.125 cm^3/cm^3 ($\psi_{soil} = -23{,}608$ cm), D_s increased by more than eightfold at the C_m of 7.5 mg/g compared to the control. This was attributed to increased water retention and improved liquid connectivity. In sandy soil, mucilage increased θ_v only at higher content but decreased D_s due to an increased liquid viscosity, which impeded solute mobility. Sandy loam showed intermediate behaviour.

Conclusion Mucilage modulates both soil water retention and nutrient diffusion in a texture-dependent manner. Its beneficial effects are most pronounced in finer-textured soils, while coarser soils require higher mucilage contents to observe similar improvements.

Keywords Mucilage exudation · Plant-soil interactions · Rhizosphere processes · Soil diffusion coefficient · Soil hydraulic properties · Water retention in soils

Responsible Editor: Tiina Roose.

Supplementary Information The online version contains supplementary material available at https://doi.org/10.1007/s11104-025-08046-6.

B. Hosseini (✉) · M. Cheraghi · D. S. Moser · M. Zarebanadkouki
Soil Biophysics and Environmental Systems, Technical University of Munich, Freising 85354, Germany
e-mail: bahareh.hosseini@tum.de

M. Cheraghi
Department of Soil Science, University College of Agriculture and Natural Resources, University of Tehran, Tehran, Iran

M. Holz · V. Pusch · R. Remus
Leibniz Centre for Agricultural Landscape Research (ZALF), Müncheberg, Germany

Introduction

Soil moisture is a critical factor influencing plant nutrient uptake, as it regulates mass flow and diffusion, the key processes governing nutrient transport to the root surface (Barber et al. 1963; Raynaud and

Leadley 2004). The rhizosphere, a narrow yet biologically and chemically active zone surrounding the root, extends only a few millimetres from the root surface but plays an extremely important role in nutrient dynamics. It is shaped by complex interactions among plant roots, soil microorganisms, and root-derived compounds such as mucilage and exudates (Philippot et al. 2013). Roots act as key modifiers of the rhizosphere environment, influencing both chemical gradients and nutrient availability within this zone. As soil moisture decreases, root water uptake becomes constrained due to the nonlinear decline in soil hydraulic conductivity, which in turn limits nutrient transport through mass flow. The reduced delivery of nutrients to the rhizosphere, combined with continued root water uptake, which further dries the surrounding zone, leads to the formation of a localized nutrient depletion area in the soil. This creates a concentration gradient that drives diffusion from the nutrient-rich bulk soil toward the rhizosphere to sustain nutrient supply to the root surface (Seiffert et al. 1995). However, declining soil moisture hampers this diffusive transport by disrupting the continuity of liquid-phase pathways that are essential for solute movement, while increasing tortuosity in the remaining connected liquid phase (Moldrup et al. 2001; Chou et al. 2012). At a critical moisture threshold, the loss of liquid-phase continuity causes a sharp decline in the soil's effective diffusion coefficient. Simultaneously, soil drying reduces the hydraulic continuity provided by liquid films and bridges linking the root surface to the surrounding soil solution, further impairing diffusion-based nutrient acquisition. The combined effects of decreased mass flow, impaired diffusion, and reduced root-soil hydraulic connectivity pose significant limitations to nutrient uptake under dry conditions, ultimately leading to nutrient deficiencies and reduced plant growth (Seiffert et al. 1995; Moldrup et al. 2001; Chou et al. 2012; Zarebanadkouki et al. 2019).

Plants have evolved several strategies to overcome these constraints and optimize nutrient uptake. One common strategy is the development of extensive root systems (Lynch 2013), which increase the volume of soil explored by roots. In addition to deeper and more branched roots, some plants invest in finer root systems and root hairs that enhance the surface area for nutrient absorption (Bienert et al. 2021; Rongsawat et al. 2021; Hosseini et al. 2024). Another strategy involves symbiotic relationships with mycorrhiza fungi, which extend the effective root zone and improve access to otherwise unavailable nutrients (Ortas and Ustuner 2014). In addition to structural modifications, plants can adjust the rhizosphere's physical and chemical properties, directly influencing nutrient availability and uptake (Holz et al. 2024b). One particularly important adaptation involves the release of root exudates, among which mucilage is considered to play a supportive role under soil drying conditions.

Mucilage is a gel-like substance composed primarily of polysaccharides and phospholipids, secreted from root tips and covering the root surface (McCully and Boyer 1997). A growing body of work shows that mucilage strongly modulates rhizosphere hydraulics, particularly under drought stress (Carminati et al. 2010; Carminati 2013; Zarebanadkouki et al. 2016; Hayat et al. 2021; Williams et al. 2021; Abdalla et al. 2024). During a soil drying cycle, it has been shown that the rhizosphere stays wetter than the surrounding bulk soil. In contrast, it has been shown that the rhizosphere turns temporarily hydrophobic upon a soil drying cycle and subsequent rewetting cycle, attributed to the presence of amphiphilic compounds in the mucilage, such as phospholipids (Moradi et al. 2012; Zarebanadkouki et al. 2016). Mucilage's intrinsic water-holding capacity is a key property that influences water retention. Mucilage comprises hydrophilic polysaccharides that can retain significant quantities of water, even under low matric potentials (Read and Gregory 1997). For instance, Benard et al. (2021) reported that pure mucilage extracted from maize seedlings could retain up to 28 g of water per gram of dry mucilage at a matric potential of −1 MPa. This intrinsic capacity to retain water enhances moisture levels in the rhizosphere, enabling soil near the roots to retain moisture even as bulk soil dries (Moradi et al. 2011; Ahmed et al. 2014; Adamczewski et al. 2024). This preserves liquid-phase continuity, which is essential for both mass flow and diffusion-driven nutrient transport.

Beyond moisture retention, mucilage also modifies water redistribution within the soil pore network, influencing liquid-phase connectivity (Benard et al. 2019; Williams et al. 2021). These effects arise from mucilage's distinct physical properties, including high water-holding capacity, low surface tension, and increased viscosity (Read and Gregory 1997;

Naveed et al. 2019; Benard et al. 2021). These properties were shown to be mucilage content dependent. Benard et al. (2019) and Williams et al. (2021) demonstrated that, unlike pure water, which drains rapidly during soil drying, mucilage delays capillary break up by enhancing liquid-phase viscosity, thereby maintaining connectivity within soil pores. Additionally, Benard et al. (2019) demonstrated that mucilage modifies the spatial distribution of water in drying soil, enabling the formation of stable capillary bridges. These bridges help retain water within soil pores, ensuring that liquid pathways remain open for nutrient diffusion and water transport (Carminati et al. 2017; Benard et al. 2019).

The degree to which mucilage impacts soil hydraulic properties and the continuity of the liquid phase depends on its content, its chemical composition, and the soil texture (Naveed et al. 2017; Kroener et al. 2018). Kroener et al. (2018) conducted a detailed investigation into the impact of mucilage extracted from chia seeds on the hydraulic properties of various soil textures. Their findings highlighted that the effects of mucilage are both content- and texture-dependent. In fine-textured soils, such as loam and clay, lower contents of mucilage were sufficient to significantly enhance soil water retention, whereas, in coarse-textured soils, like sand, higher contents were required to observe similar benefits. This difference was primarily attributed to the larger pore spaces in sandy soils, which require a more viscous mucilage to bridge across larger pores and avoid capillary breakup (Benard et al. 2021). Similarly, Zarebanadkouki et al. (2019) demonstrated that incorporating chia seed mucilage into washed quartz sand enhanced the effective nutrient diffusivity of ^{137}Cs, especially under low soil water contents, and improved the simulated potassium uptake by plant roots. Chenu & Roberson (1996) also reported an increased diffusion of glucose in xanthan-amended kaolinite.

While these studies have provided valuable insights into the role of mucilage in improving soil transport properties, they are limited by either their use of simplified systems involving single soil texture or washed quartz sands or using a model substance mucilage. This leaves critical knowledge gaps regarding the behaviour of plant-derived mucilage across a range of natural soil textures, where pore structures are more complex and heterogeneous. Additionally, the interplay between mucilage content, soil moisture levels, and nutrient diffusion in diverse soil textures is not yet fully understood. Addressing these gaps is essential for understanding how mucilage modulates rhizosphere processes in real-world conditions.

This study aimed to address these knowledge gaps by investigating the role of plant-derived mucilage in modifying soil water retention and nutrient diffusion across different soil textures and moisture levels. We specifically focused on the effective diffusion coefficient (D_s), a key parameter that describes nutrient movement through soil and is influenced by pore structure and tortuosity. We employed phosphor imaging to quantify the diffusion of radioactively labelled Calcium (^{45}Ca). Additionally, we introduced the soil-specific impedance factor (f), which governs nutrient diffusion in soil, and considered the impact of mucilage on it in different aspects.

Methods and materials

Mucilage collection

The maize seed variety KWS EDITO was cultivated following an adaptation of the method developed by Zickenrott et al. (2016).The seeds were first sterilized in 10% H_2O_2 for 10 min and were then germinated on a polyamide mesh (1 mm mesh size) positioned 30 cm above the bottom of polyethylene boxes (dimensions: 40 cm height, 60 cm length, and 40 cm width). The box was filled with water to a height of 10 cm, sealed, and kept in darkness. A porous ceramic plate (40×4 cm^2) was installed at the bottom of the boxes to provide controlled airflow, creating air bubbles and maintaining high humidity levels within the enclosed space, which optimized conditions for seed germination and prevented the exuded mucilage dehydration. After three to four days, once the seedlings roots reached a length of 3–5 cm, the mucilage was collected using a suction pump set to approximately –200 hPa. The collected mucilage was then filtered through a 200-micron sieve, and its concentration was determined by calculating the ratio of the oven-dry weight of the mucilage to its initial wet weight.

Experimental setups and treatments

The experimental design included three soil textures (sand, sandy loam, loam) and four mucilage

contents (C_m) of 0.0, 2.5, 5.0, and 7.5 [mg dry mucilage g dry soil], simplified as mg/g throughout the text. These were tested at three levels of soil water content (θ_v) of 0.30, 0.20, and 0.125 cm^3 liquid/cm^3 soil which simplified as cm^3/cm^3 through the text. The tested soil textures were: i) pure sandy soil sieved between 630–63 µm, ii) a sandy loam soil consisting of 65% sand, 34.95% silt, and 0.05% clay, iii) a loam soil consisting of 36% sand, 40% silt, and 24% clay. The soil organic matter was removed by heating soils in a muffle furnace to a temperature of 500–600°C. To prepare the rhizosphere analog soils, the extracted mucilage was mixed with soil at contents (C_m) of 0.0, 2.5, 5.0, and 7.5 mg/g. To ensure uniform mixing, we first diluted the required amount of mucilage for each treatment in distilled water, adjusting the solution to achieve a θ_v of 0.35 cm^3/cm^3 upon mixing with soil by the addition of distilled water. The mucilage solution was then thoroughly mixed with the soil to ensure homogeneous distribution. Finally, the prepared mixture was gradually air-dried to the target water content required for the diffusion experiment while it was continuously mixed to avoid the development of local soil drying and mucilage accumulation at the soil surface.

Effect of mucilage on soil water retention

The soil water retention curves ($\theta_v(\psi_{soil})$) for the three selected soil textures, each mixed with four mucilage contents, were determined using a combination of the sandbox and sand-kaolin box methods for water potentials ranging from 0 to –300 cm, followed by the pressure plate method for potentials from –1000 to –15,000 cm. The rhizosphere analog soils were packed into containers (2.15 cm in diameter, 0.8 cm in height) at a predetermined bulk density and saturated for 48 h using a slow wetting technique to minimize air entrapment. Water potential was gradually reduced, and the corresponding θ_v was measured gravimetrically at equilibrium, confirmed by stable weight over two days (Kroener et al. 2018). The Van Genuchten (VG) model was applied to fit the data and generate the retention curves (Van Genuchten 1980). All measurements were performed in triplicate.

Quantification of calcium diffusion: phosphor imaging technique

The diffusion experiment was designed to assess the effect of varying mucilage contents on calcium (^{45}Ca) transport across different soil textures under controlled moisture levels. The rhizosphere analog soils were divided into two subgroups. One subgroup was rewetted with distilled water to θ_v of 0.35 cm^3/cm^3, while the other was rewetted to the same θ_v using a 60 mM $CaCl_2$ solution labelled with 8 MBq of $^{45}CaCl_2$. After wetting, both subgroups were gently but continuously mixed and air-dried to the target of θ_v of 0.30, 0.20, or 0.125 cm^3/cm^3. Continuous mixing prevented the formation of locally desiccated zones or salt crusts at the sample surface. This preparation procedure ensures that (i) the total radiotracer activity in each sample remains consistent (per volume of soil) regardless of moisture content and (ii) a higher concentration of $^{45}CaCl_2$ in the liquid phase of soils dedicated to lower water content treatment was achieved to facilitate the diffusion process.

After reaching the targeted water content, the soil was covered and kept in a cool place at a temperature of 4 °C for 24 hr to equilibrate in water content. Following equilibration, the first half (2.5 cm) of PVC-made containers (5 cm × 1 cm × 0.3 cm) was filled with the radiotracer-treated soil, while the other half was packed with the corresponding soil treatment moistened only with distilled water. To maintain a sharp boundary between the compartments, a solid cubic block (2.5 cm × 1 cm × 1 cm) was placed inside the containers while packing the soil into the first compartment. The containers were then sealed with transparent plastic covers to prevent evaporation, fixed on pre-designed plates, and stored under vapour-saturated conditions at a constant temperature of 20 °C for 65 days. The containers were placed horizontally during the experiment to prevent any mass flow driven by gravity.

Phosphor imaging (Holz et al. 2019, 2024a) was used to track the spatiotemporal distribution of ^{45}Ca at 10 intervals over 65 days (e.g., 0, 48, 217, 383 hr). In this method, samples containing ^{45}Ca were placed in contact with a storage screen (BAS-IP MS 2024 E, VWR) in the dark for 2 h, and the energy from the radioactive decay was stored. After exposure, the screens were scanned using a laser scanner (Amersham Typhoon IP) to generate high-resolution (50 µm) digital images. The resulting digital images were processed using the ImageQuantTL software to generate intensity profiles with a unit of PSL (Photo Stimulated Luminescence, a standard unit in ImageQuantTL), which were then converted into ^{45}Ca activity based on predetermined calibration curves (detailed in the next section). Finally, the activity was converted into Ca concentration [mg] using

a pre-determined time-dependent conversion factor (CF with a unit mg Ca/kBq). The CF was initially defined as the ratio of Ca concentration [mg] to activity [kBq] in the stock solution. To account for the radioactive decay of ^{45}Ca, a different conversion factor was applied at each measurement time. This was achieved by correcting the initial activity of ^{45}Ca in the stock solution for radioactive decay, using the known decay constant of ^{45}Ca (2.96×10^{-6} [1/hr]). This approach ensured that Ca concentrations were accurately adjusted over time, compensating for the gradual decrease in activity due to decay.

Determination of calibration function

To convert the PSL profiles from phosphor imaging into ^{45}Ca activity, a calibration function was established for each soil texture and moisture level. For this purpose, rhizosphere analog soils were mixed with solutions containing six known activities of ^{45}Ca, ranging from 0.025 to 8 MBq/mL. Each soil mixture was then adjusted to the target θ_v levels of 0.30, 0.20, and 0.125 cm^3/cm^3, followed by stepwise drying. To determine the exact activity of each radiotracer solution, 100 µL samples were mixed with 6 mL of ROTISZINT Eco High (Roth, Germany, Art. No. 1 P1C.2) and measured using a liquid scintillation counter (TriCarb 2900 TR, PerkinElmer, Germany). The soil samples were then packed into containers (2.5 cm×1 cm×0.3 cm) and imaged using the phosphor imaging technique, following the same procedure as in the main experiment. The resulting PSL values for each known activity were then plotted against the known ^{45}Ca activities. Our results did not indicate a significant effect of varying soil water contents on the PSL obtained within a given soil texture; therefore, we pooled all data of different water contents together. A linear regression function was fitted to the relationship between PSL and activity data, generating a calibration curve specific to each soil texture. This function was subsequently used to convert the intensity profiles from the main diffusion experiment into ^{45}Ca activity (Fig. S1).

Modeling calcium transport to estimate diffusion coefficients

The diffusive transport of Ca within our soil system (uniform soil properties and soil water content (θ_v) in time and space) was described by a diffusion equation as follows:

$$\left(\theta_v + \rho_b K_d\right)\frac{\partial C_w}{\partial t} = D_s\left(\frac{\partial^2 C_w}{\partial x^2}\right) \quad (1)$$

where C_w is the concentration of Ca per volume of soil liquid [mg/cm^3 soil liquid], t is time [hr], D_s is the effective diffusion coefficient of Ca in soil [cm^3 soil liquid/cm^1 soil hr], ρ_b is the soil bulk density [g soil/cm^3soil], and K_d is the soil partition coefficient [cm^3 liquid/g soil]. Here, we assumed linear and rapid equilibration between the concentration of dissolved Ca in the liquid phase and the adsorbed Ca on the solid phase. The parameter K_d was fixed based on experimentally measured values. The term $C_w\left(\theta_v + \rho_b K_d\right)$ on the left side of Eq. (1) represents the total concentration of Ca [mg/cm^3 soil] accounting for Ca in both the liquid and solid phases. This is determined through time-series images obtained via phosphor imaging. The term on the right describes 1D diffusive transport of Ca within the soil driven by the concentration gradient in the soil liquid.

Equation (1) was discretized using an implicit numerical scheme and then solved numerically in Python 3.9. The fitting process aimed to minimize the difference between the simulated and measured concentration profiles by optimizing D_s. The inverse modeling was conducted using the observed Ca concentration profiles across the unlabelled section of the container positioned 0.5 cm away from the border between the two compartments. This choice was made to exclude potential discontinuities at the interface between the labelled and unlabelled soil compartments, impacting the diffusion of Ca across the soil domain. To solve Eq. (1) numerically, we used a known initial concentration of $C_t(x, t_0)$, which was obtained from the result of the first phosphor imaging measurement taken at time zero (t_0). In addition, we assumed a no-flux boundary condition (BC) at the end of the domain (the far end of the unlabelled compartment) and a variable concentration BC at the start of the simulation domain, representing the labelled compartment formulated as

$$\left.\frac{\partial C_t}{\partial x}\right|_{x=L} = 0 \quad (2a)$$

$$C_t(x = 0, t) = C_{labelled}(t) \quad (2b)$$

where $C_{labelled}(t)$ represents the time-dependent concentration at the labelled compartment boundary, derived from phosphor imaging data. Note that $C_t = C_w(\theta_v + \rho_b K_d)$. The objective function for minimization was defined as:

$$ObjFun = \frac{(Xmes - Xsim)^2}{Xmes^2} \quad (3)$$

where *Xmes* represents the measured Ca concentration at any time t and any position x, and *Xsim* represents the simulated Ca concentration. The optimization was performed using the lmfit library in Python (Newville et al. 2021), which adjusted the parameters needed to describe D_s as a function of soil water content and mucilage (detailed in the section below) to best match the observed profiles of Ca concentration over time and space.

Determination of soil partition coefficient

The soil partition coefficient (K_d), was determined to quantify the distribution of Ca between the liquid and solid phases in the soil. This parameter is crucial for modelling nutrient diffusion as it distinguishes the portion of Ca available for transport in the liquid phase from that adsorbed onto soil particles. Additionally, it provides insight into how mucilage influences cation adsorption in soil. To determine K_d, five different concentrations of $CaCl_2$ solution (10 to 120 mM) were prepared. Four millilitres of each solution were mixed with 2 g of each prepared rhizosphere analog soil as well as control soils, without mucilage ($C_m = 0$), in pre-washed 15 mL polypropylene centrifuge tubes. The mixtures were shaken for 12 hr to achieve equilibrium and filtered through the Whatman No. 42 filter paper. These experiments were replicated twice. The Ca concentration in the liquid phase was measured using inductively coupled plasma optical emission spectrometry (ICP-OES). The difference in Ca concentration before and after equilibration was used to calculate the amount of Ca adsorbed onto the solid phase. The relationship between Ca concentrations in the liquid (C_w) and solid phases (C_S) was fitted using the linear function below to obtain K_d

$$C_s = K_d C_w \quad (4)$$

where K_d is the soil partition coefficient [cm^3liquid/g soil], C_w is the concentration of Ca in the liquid phase [mg/cm^3liquid], and the C_s is the absorbed amount of Ca in the solid phase of dry soil [mg/g soil]. We elected to use a linear partitioning (K_d) relationship because, within the concentration range investigated in our experiment, the measured Ca concentration in the liquid phase and the corresponding sorbed Ca on the solid phase showed a linear relation ($0.63 < R^2 < 0.99$ among all treatments). In other words, the data showed no nonlinearity that would justify introducing additional fitting parameters (e.g., Freundlich exponent or Langmuir plateau) (Table 1).

Modelling the overall impact of mucilage on the diffusion coefficient of rhizosphere

In this study, we experimentally determined the impact of mucilage on D_s at three selected θ_v to specifically assess its role in redistributing and maintaining liquid-phase connectivity, independent of its impact on soil water retention. However, mucilage also alters the soil water retention curve ($\theta_v(\psi_{soil})$ relationship), which must be integrated to fully evaluate its overall influence on D_s. To address both effects, we employed a two-step modelling framework.

Step 1: Develop a conceptual model linking the dynamics of D_s to mucilage content and soil water content (θ_v), explicitly incorporating mucilage's effects on the tortuosity-connectivity of water-filled pore pathways.

Step 2: Use measured $\theta_v(\psi_{soil})$ data for mucilage-treated soils to convert $D_s(\theta_v)$ to $D_s(\psi_{soil})$, establishing an analysis of nutrient diffusion dynamics across realistic rhizosphere moisture conditions, including the overall effect of mucilage on D_s.

Step 1: Conceptual Model for $D_s(\theta_v)$

Inspired by Ghanbarian et al. 2015, the effective diffusion coefficient under partially saturated conditions (D_s) in pure medium is expressed as:

$$D_s(\theta_v, C_{m,l}) = D_s(\theta_s, C_{m,l}) \times f_v(\theta_v, C_{m,l}) \times f_l(\theta_v, C_m) \quad (5)$$

where the $D_s(\theta_v, C_{m,l})$ is the effective diffusion coefficient in soil [cm^3 soil liquid/cm^1 soil hr], which is simplified to [cm^2/hr] throughout the text, $C_{m,l}$ is the apparent mucilage content in the liquid phase [mg dry mucilage/cm^3 liquid], $D_s(\theta_s, C_{m,l})$ is the effective

Table 1 Summary of terms and their units

Term	Definition	Unit of measurement
C_t	The total concentration of Ca per soil volume	mg/cm^{3}soil
C_w	The total concentration of Ca in the liquid phase	mg/cm^{3}liquid
C_s	The total concentration of Ca in the solid phase	mg/g soil
C_m	Mucilage content	mg dry mucilage/g dry soil
$C_{m,l}$	Apparent mucilage content in liquid phase	mg dry mucilage/cm^3 liquid
θ_v	Volumetric water content	cm^{3}liquid/cm^{3}soil
θ_s	Saturated water content	cm^{3}liquid/cm^{3}soil
θ_r	Residual water content	cm^{3}liquid/cm^{3}soil
φ	Soil porosity	cm^{3}liquid/cm^{3}soil
ρ_b	Soil bulk density	g soil /cm^{3}soil
K_d	Soil partition coefficient	cm^{3}liquid/g soil
ψ_{soil}	Soil matric potential	cm
n	Van Genuchten parameter	−
α	Van Genuchten parameter	1/cm
D_s	Soil effective diffusion coefficient	cm^{3}soilliquid/cm^{1}soil hr
$D_s(\theta_s)$	Soil effective diffusion coefficient at saturation	cm^{3}soil liquid/cm^{1}soil hr
D_0	Diffusion coefficient of calcium in pure water	cm^2/hr
f_v	Viscosity-induced impedance factor	−
f_l	Tortuosity-induced impedance factor	−
μ_w	Water viscosity	mPa. s
μ_m	Bulk viscosity of a water-mucilage mixture	mPa. s
$\mu_{m,dif}$	Diffusional viscosity of mucilage	mPa. s
C_0	Fitting parameter	mg/cm^3 liquid
C_1	Fitting parameter	mg/cm^3 liquid
d_0	Fitting parameter	−
d_1	Fitting parameter	−
β	Mucilage viscosity scaling factor	−
λ	soil tortuosity-connectivity factor	−
a	Fitting Parameter	−
b	Fitting Parameter	−
c	Fitting Parameter	g dry soil/mg dry mucilage
d	Fitting Parameter	g dry soil^2/mg dry mucilage^2

diffusion coefficient in fully saturated soil [cm^2/hr], $f_v(\theta_v, C_{m,l})$ is the impedance factor associated with the effect of mucilage viscosity [-],$f_l(\theta_v, C_m)$ is the impedance factor arising from the tortuosity and connectivity of the diffusive path in soils [-], and C_m is mucilage content expressed as mg dry mucilage per g of dry soil. The apparent mucilage content in the liquid was estimated according to the equation below:

$$C_{m,l} = \frac{C_m \times \rho_b}{\theta_v} \tag{6}$$

where, C_m is mucilage content expressed as mg dry mucilage per g of dry soil, ρ_b is soil bulk density [g soil/cm^{-3}soil], and θ_v is the soil water content [cm^3/cm^3]. It is important to note that this expression represents an *apparent* mucilage content in the soil solution. The true content experienced by solutes may differ because part of the mucilage can adsorb to soil particle surfaces, become entrapped in micro-pores, or interact physically and chemically with the soil matrix. Nevertheless, the apparent content provides a tractable first-order approximation for parameterizing mucilage effects on effective diffusion.

The formulation in Eq. (5) enables us to express the D_s, as a joint function of θ_v and $C_{m,l}$ by explicitly capturing the mechanistic pathways through which mucilage modulates each process that governs nutrient diffusion in soil, as detailed below:

i) Mucilage Viscosity-driven Effect

Mucilage strongly alters the physical properties of the soil solution, most prominently its viscosity. Kroener et al. (2014) proposed a stretched-exponential formulation for the effective flow viscosity (μ_m) of mucilage–water mixtures as a function of mucilage concentration as follows

$$\mu_m = max\begin{cases} \left(\frac{C_{m,l}}{C_0}\right)^{d_0} + \mu_w \\ \left(\frac{C_{m,l}}{C_1}\right)^{d_1} \end{cases} \quad (7)$$

where μ_w [mPa. s] is the viscosity of pure water, $C_{m,l}$ [mg dry mucilage/cm^3 liquid] is the apparent mucilage content in the liquid phase, and d_0, d_1, C_0, and C_1 are empirical constants derived from rheological measurements. To determine the values of d_0, d_1, C_0, and C_1, Eq. (7) was fitted to experimentally measured viscosity data as a function of maize mucilage content reported by Benard et al. (2021), as shown in Fig. S2. The optimal parameter values were identified as d_0= 3.5162, d_1= 2.0456, C_0= 0.3044, and C_1= 0.8812. Because these measurements are based on bulk rheometry, μ_w describes the viscous resistance experienced by the entire mucilage-water mixture during macroscopic flow. However, solute diffusion through mucilage occurs at the microscale, where solutes move through water-filled channels within the polymer network. Experimental and theoretical studies on probe diffusion in polymer solutions (Phillies 2007) show that the effective viscosity perceived by diffusing molecules ("microviscosity") is typically smaller than the bulk viscosity, as Brownian motion is only partially hindered by the polymer matrix. In other words, diffusing solutes experience a screened hydrodynamic drag rather than the full macroscopic resistance. To account for this, we introduced a diffusional effective viscosity ($\mu_{m,dif}$), which retains the same functional form as μ_m but is scaled in magnitude to represent the hydrodynamic resistance relevant for solute diffusion:

$$\mu_{m,dif} = \mu_m{}^{\beta} \quad (8)$$

where β is a dimensionless scaling factor ($0 < \beta < 1$) that attenuates the viscosity experienced by solutes relative to the macroscopic mucilage-water mixture. This formulation assumes that the shape of the viscosity–concentration curve remains unchanged, but its intensity is weakened for diffusion processes.

Finally, following the Stokes–Einstein relation, the viscosity impedance factor (f_v) representing diffusional hindrance in Eq. (5) can be written as:

$$f_v = \left(\frac{\mu_w}{\mu_{m,dif}}\right) \quad (9)$$

ii) Liquid connectivity enhancementLiquid connectivity enhancement

Even at the same water content, mucilage may still modify the connectivity of water-filled pathway by altering the redistribution of water within soil (Benard et al. 2019; Williams et al. 2021). This is modelled by defining the term f_l in Eq. (5) as follows (Ghanbarian et al. 2015):

$$f_l = \left(\frac{\theta_v - \theta_r}{\phi - \theta_r}\right)^{\lambda} \quad (10)$$

where θ_v is the soil water content [cm^3/cm^3], θ_r is the residual water content [cm^3/cm^3], obtained from the fitted Van Genuchten (VG) model applied to soil water retention data (Table 2), ϕ represents the soil porosity, corresponding to the saturated water content θ_s [cm^3/cm^3], also derived from the fitted VG model (Table 2); and λ is the soil tortuosity-connectivity factor [-], defined as follows:

$$\lambda = a + \frac{b}{1 + (cC_m + dC_m^2)^2} \quad (11)$$

where, a$\geq$0 [-], b [-], c [g dry soil/mg dry mucilage], and d [g dry soil^2/mg dry mucilage^2] are fitting parameters and C_m is mucilage content [mg dry mucilage/g dry soil]. This four-parameter Lorentzian-type rational function [-] ensures a smooth, monotonic decline of λ without crossing

Table 2 Soil hydraulic properties of soils treated with varying contents of mucilage

Soil texture	C_m $[\frac{mg}{g}]$	θ_s $[\frac{cm^3}{cm^3}]$	θ_r $[\frac{cm^3}{cm^3}]$	α $[\frac{1}{cm}]$	n [−]
Sand	0	0.41 ± 0.01	0.02 ± 0.004	0.14 ± 0.10	1.74 ± 0.18
	2.5	0.46 ± 0.01	0.01 ± 0.003	0.15 ± 0.10	1.67 ± 0.12
	5.0	0.43 ± 0.02	0.01 ± 0.003	0.08 ± 0.06	1.88 ± 0.27
	7.5	0.39 ± 0.06	0.01 ± 0.003	0.02 ± 0.01	1.93 ± 0.19
Sandy loam	0	0.49 ± 0.02	0.05 ± 0.013	0.06 ± 0.02	1.37 ± 0.05
	2.5	0.49 ± 0.02	0.03 ± 0.013	0.35 ± 0.13	1.25 ± 0.03
	5.0	0.50 ± 0.01	0.01 ± 0.011	0.27 ± 0.07	1.25 ± 0.02
	7.5	0.49 ± 0.03	0.01 ± 0.046	0.18 ± 0.13	1.22 ± 0.06
Loam	0	0.54 ± 0.03	0.01 ± 0.102	0.07 ± 0.06	1.20 ± 0.01
	2.5	0.58 ± 0.02	0.01 ± 0.052	0.08 ± 0.03	1.22 ± 0.05
	5.0	0.59 ± 0.05	0.01 ± 0.260	0.21 ± 0.35	1.14 ± 0.12
	7.5	0.64 ± 0.06	0.01 ± 0.256	0.28 ± 0.48	1.14 ± 0.12

C_m mucilage content, θ_s saturated water content, θ_r residual water content, α air entry point, and n steepness of retention curve

These parameters were determined by fitting the measured soil retention curve data using the VG model alongside their standard errors

zero, while remaining sufficiently flexible to reproduce both texture-dependent and mucilage-dependent behaviour of λ.

The concept, introduced in Eq. (5) integrates mechanistic processes governing mucilage impact on D_s of nutrients, including viscosity-driven resistance and the effects of liquid-phase tortuosity-connectivity. However, while the underlying mechanisms are based on physical principles, their parameterization remains empirical due to the complexity of directly quantifying mucilage behaviour in soil.

Step 2: Evaluation of the overall effect of mucilage on D_s by linking $D_s(\theta_v)$ to $D_s(\psi_{soil})$

To further explore the combined effect of mucilage on nutrient diffusion, we first estimated θ_v of soils mixed with varying mucilage contents across a predefined range of soil matric potentials (ψ_{soil}). Then the fitted conceptual model (Eq. (5)) and its parameters were used to predict D_s across the respective range of ψ_{soil}. This procedure allowed us to convert $D_s(\theta_v)$ to $D_s(\psi_{soil})$.

Data processing and statistical analysis

For the water retention experiment, the matric potentials of the control soils, corresponding to water contents (θ_v) of 0.30, 0.20, and 0.125 cm^3/cm^3, were determined for each soil texture. Subsequently, the θ_v values of rhizosphere analog soils corresponding to these reference matric potentials were extracted from the relevant retention curve. A one-way ANOVA (James et al. 2023) was conducted with θ_v as the response variable and mucilage content (C_m) as the factor (with 4 levels) for each corresponding matric potential (ψ_{soil}), separately for each soil texture. After verifying the normality of the residuals using the Shapiro–Wilk test performed with the stats module from the SciPy library (Virtanen et al. 2020), we used Tukey's HSD test (James et al. 2023) to determine significant differences between the mean values of θ_v across different levels of C_m for each ψ_{soil}.

For the diffusion experiment, a one-way ANOVA (James et al. 2023) was conducted to evaluate the effect of C_m as a factor with 4 levels on the response variable of effective diffusion coefficient (D_s) across θ_v for each soil texture. This analysis was implemented using the Statsmodels library in Python (Seabold and Perktold 2010). To meet the assumptions of normality and homogeneity of residual, log transformations were applied to D_s prior to further analysis. Residual normality was assessed using the Shapiro–Wilk test (Virtanen et al. 2020), and significant differences between group means were evaluated using Tukey's HSD test (James et al. 2023), implemented via the statsmodels.stats.multicomp module in Python (Seabold and Perktold 2010). All statistical tests were conducted at a significant level of $\alpha = 0.05$. All figures were generated using Python 3.9.

Results

Effect of mucilage on soil water retention

Figures 1a, b, and c display the measured and modelled water retention curves for sand, sandy loam, and loam, respectively. The corresponding fitted parameters of the VG model are detailed in Table 2. As shown in Fig. 1, the impact of mucilage on soil water-holding capacity was strongly influenced by soil texture. To thoroughly assess the effect of mucilage on water retention within the rhizosphere analog soils, the matric potentials corresponding to the water content used in the experiments are plotted alongside the water retention curves (Fig. 1d, e, and f).

Sandy soil treated with mucilage showed higher water content at each matric potential than control soil. However, statistically significant differences were observed only at the highest mucilage content (C_m = 7.5 mg/g) and at the most negative matric potential (ψ_{soil} = − 37 cm). Indeed, the θ_v was enhanced by a factor of two in rhizosphere analog soil compared with control soil (θ_v of 0.12 vs 0.25 cm^3/cm^3). However, an increased water content trend was observed only at the highest mucilage concentration across the three selected soil matric potentials in sandy loam. Nevertheless, this increase was not statistically significant (Fig. 1e). In the case of loam soil, both the C_m of 7.5 and 5.0 mg/g resulted in significantly higher θ_v in the analog rhizosphere soil compared with the control. This enhancement was approximately 1.5 times greater at ψ_{soil} of − 23,608 cm, 1.3 times greater at ψ_{soil} of − 2426, and 1.2 times greater at ψ_{soil} of − 266 cm compared to the control soil at both C_m.

Effect of mucilage on soil diffusion coefficient

Figure 2 illustrates exemplary imaging of ^{45}Ca diffusion in a selected soil texture (loam) at the lowest chosen soil water content (θ_v= 0.125 cm^3/cm^3) affected by four different C_m over time (days). The accompanying colour map represents the as grey values intensity in captured images, where darker blue areas represent high and pale green areas indicate very low ^{45}Ca activities. Over time (days), ^{45}Ca diffused from the labelled compartment (dark blue, labelled with $^{45}CaCl_2$) to the unlabelled compartment, driven by the concentration gradient. To further illustrate the redistribution of Ca during diffusion, we compared concentration profiles between an early stage (100 hr) and a late stage (820 hr) of the experiment (Fig. 2c). The resulting difference profile represents the net change in tracer activity over this 720-hr interval (≈30 days). Positive values indicate zones where ^{45}Ca accumulated relative to the initial state, whereas negative values indicate depletion. This approach does not reflect instantaneous fluxes, but instead provides a simple measure of net transport and redistribution, making it possible to directly compare diffusion dynamics across treatments.

Comparing ^{45}Ca transport in soils with and without mucilage revealed that mucilage enhanced ^{45}Ca movement in treated soils compared to untreated ones (Fig. 2b and c). As time progressed, at Day 21 onwards, the solute front in the 7.5 mg/g treatment advanced further than the control and the other treatment, indicating an overall enhancement of diffusion (Fig. 2b and c).

Figure 3 shows the profiles of the Ca concentrations as the function of distance at various times (hr) for exemplary samples shown in Fig. 2. Here, the profiles are shown only for the soil regions beyond the labelled compartment (Fig. 3). With time, Ca moved from the left-side (labelled part) to the right-side (unlabelled part) at varying rates (Fig. 3). Equation (1) was well fitted to the observed Ca concentration profiles by D_s inversely adjusting D_s.

The mean estimated values of D_s are shown in Fig. 4. As shown in Fig. 4, soil drying from θ_v of 0.30 to 0.125 cm^3/cm^3 decreased in D_s across all soil textures. In the absence of mucilage (C_m = 0), this soil drying led to a 2.1-fold decrease in D_s for sand, a 1.7-fold decrease for sandy loam, and a 4.6-fold decrease for loam soils. To better understand the impact of mucilage at each selected θ_v on D_s, we compared D_s of soils mixed with different levels of C_m at each specific θ_v across different soil textures.

In sand-textured soil, rhizosphere analog soils mixed with varying C_m levels showed a lower D_s compared to the control soil, especially in higher water content levels (i.e., θ_v= 0.3). Notably, in sandy soil mixed with C_m=5.0 mg/g, the D_s at all moisture levels were significantly lower than in the control (Fig. 4a). This reduction was more pronounced in wetter soil (3.4-fold decrease) compared to drier soil (3.2-fold decrease), as shown in Fig. 4a. The pattern reversed in the case of the other fine-textured soils. In sandy loam (Fig. 4b), while the presence of mucilage at almost all content levels showed

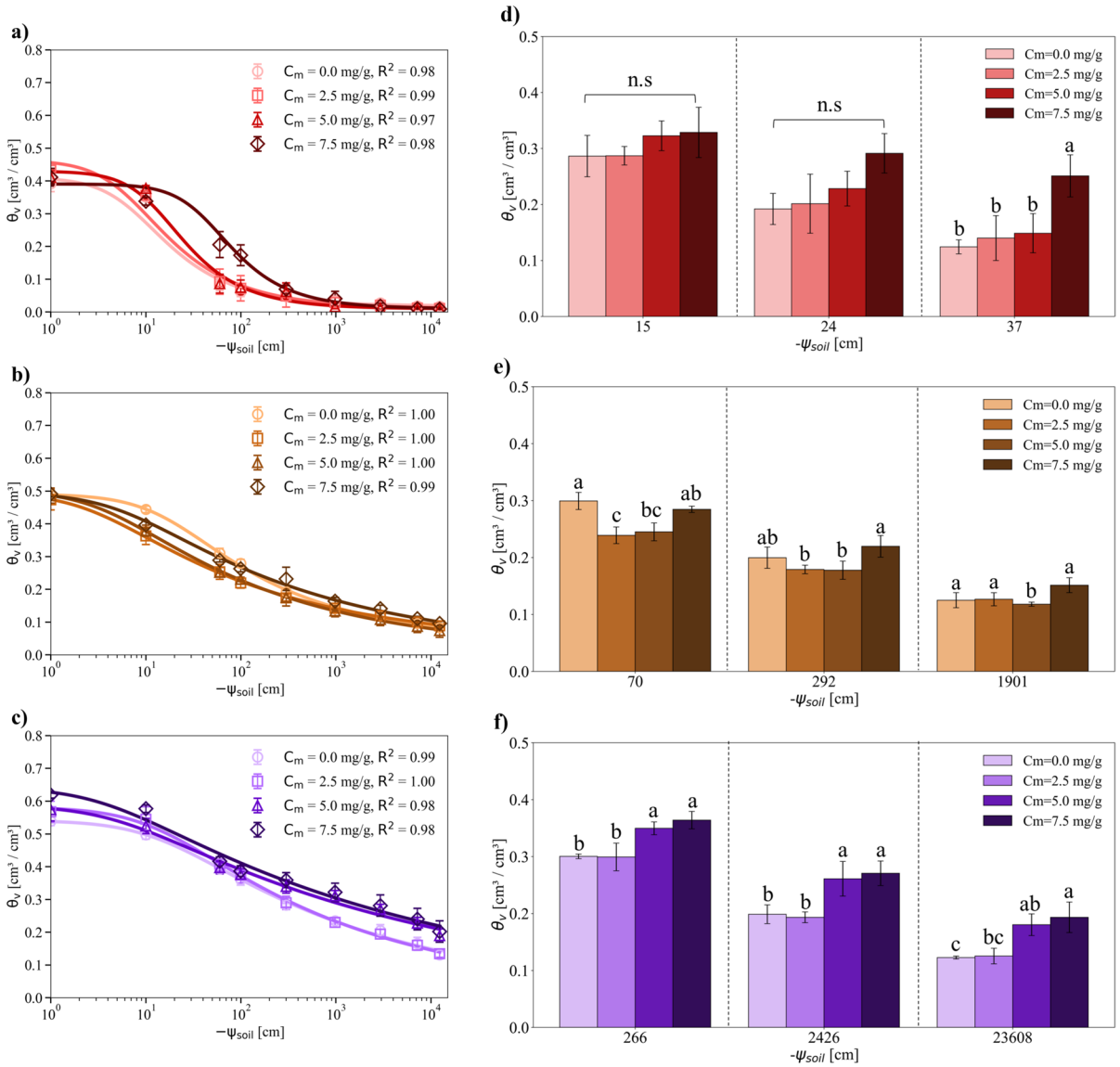

Fig. 1 Measured and fitted water retention curves of **a**) sand, **b**) sandy loam, and **c**) loam textures affected by different mucilage contents (C_m) of 0, 2.5, 5.0, and 7.5 [mg/g]. The dots refer to measured data; the lines are predicted values according to the VG model. The mean comparison of the θ_v of **d**) sand, **e**) sandy loam, and **f**) loam textures affected by C_m of 0, 2.5, 5.0, and 7.5 [mg/g] at each ψ_{soil} corresponding to θ_v of 0.30, 0.20, and 0.125 [$cm^3/cm.^3$] of control soil (C_m of 0). Data are the average of 3 replications, and the error bars indicate the standard deviation. Different letters indicate significant differences ($\alpha < 0.05$)

an increasing trend in D_s, this increase was not statistically significant. For the loam texture (the finest soil texture), both the highest and intermediate mucilage contents (C_m= 7.5 and 5.0 mg/g) resulted in noticeably higher D_s values at θ_v levels of 0.30 and compared to soil without mucilage (Fig. 4c). However, at θ_v of 0.20 and 0.125 cm^3/cm^3, all level of C_m significantly maintained a higher D_s compared to the control soil, with values of $2.4\times10^{-4}\pm4.3\times10^{-5}$ for C_m= 7.5, $1.4\times10^{-4}\pm4.9\times10^{-5}$ for C_m= 5.0, $1\times10^{-4}\pm4.6\times10^{-5}$ for C_m= 2.5 versus $2.8\times10^{-5}\pm1.7\times10^{-5}$ for C_m= 0.0, respectively in θ_v levels of 0.125 (Fig. 4c).

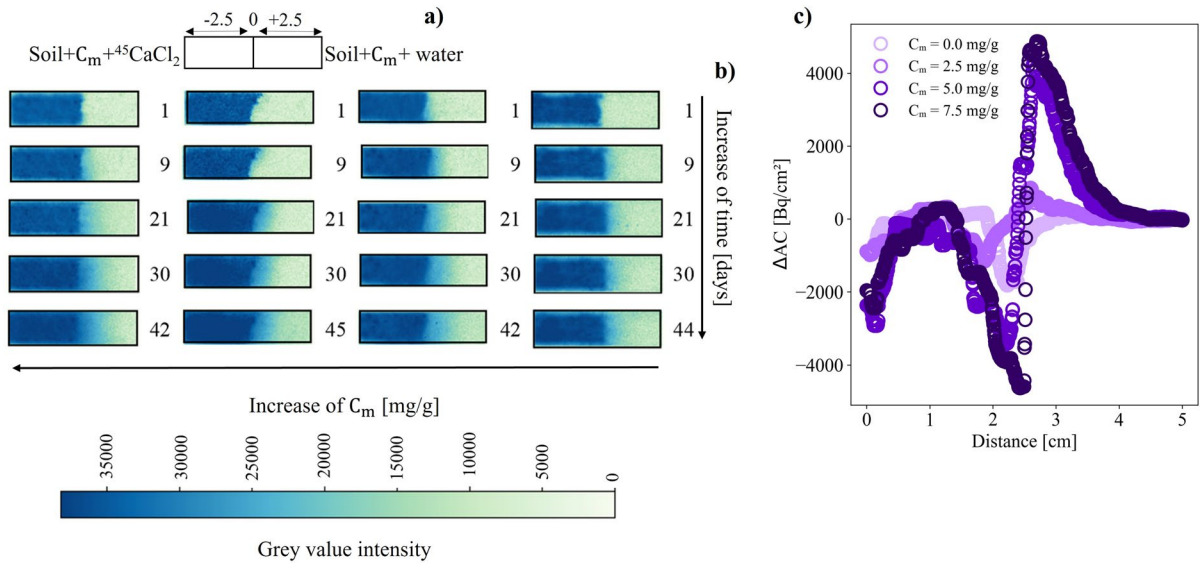

Fig. 2 **a**) Schematic of the experimental setup. The left compartment contained the ^{45}Ca-labelled solution, and the right side was wetted to the same respective water content with distilled water. **b**) Representative images of ^{45}Ca distribution in loam soil treated with varying C_m of 0, 2.5, 5.0, and 7.5 [mg/g] at different times (days). The colour map indicates grey value intensities, with dark blue representing high activity of ^{45}Ca and pale green indicating low or no activity. Note that grey values are not identical to PSL values extracted from ImageQuantTL. Each mucilage treatment was conducted in a separate batch, resulting in non-identical scanning intervals. Raw intensity values were converted to ^{45}Ca activities (AC) and then to Ca concentrations using predefined calibration factors. **c**) Net redistribution of ^{45}Ca over the diffusion period. To construct this profile, the tracer activity measured at 100 hr was subtracted from that at 820 hr for each position along the soil domain and then averaged along sample width. The resulting difference ($\Delta AC = AC_{820hr} - AC_{100hr}$) represents the net change in ^{45}Ca activity during the 720 hr interval (≈30 days). Positive values indicate soil regions where ^{45}Ca accumulated relative to the early state, whereas negative values indicate depletion. This difference plot does not capture instantaneous fluxes but instead provides a simple proxy for net transport and redistribution, facilitating direct comparison of diffusion patterns among treatments.

Overall impact of mucilage on the effective diffusion coefficient of the rhizosphere

The conceptual model presented in Eq. (5) was well fitted to the measured D_s values across three selected θ_v and C_m levels, separately for each soil texture (Fig. 4). Using this conceptual model allowed us to reproduce a continuous function describing mucilage impact at varying content on effective diffusion coefficient of each respective soil texture as a function of water content ($D_s(\theta_v)$). The optimized model parameters for each soil texture are summarized in Table 3. The derived functions were then used to link $D_s(\theta_v)$ to $D_s(\psi_{soil})$ based on the parameterized $\theta_v(\psi_{soil})$ relation in Fig. 1, and the results are plotted in Fig. 5. This conversion allows us to compare D_s of bulk soil with the emerging D_s of the rhizosphere at varying mucilage contents, assuming that both regions will be at equilibrium matric potential (for instance, at night-time).

$D_s(\theta_s)$ effective diffusion coefficient at soil water saturated condition, β viscosity scaling factor, *a, b, c, d* fitting parameters, C_m mucilage content, and K_d partition coefficient.

As illustrated in Fig. 5a, the presence of mucilage at 5.0 mg/g markedly reduced $D_s(\psi_{soil})$ in sand texture compared to the control soil across all matric potentials. At C_m = 2.5 mg/g, this reduction occurred only under wet conditions ($\psi_{soil} > -36$ cm), whereas no reduction was observed at presence of the highest mucilage content (C_m = 7.5 mg/g). Notably, at $\psi_{soil} = -100$ cm representing a dry condition in sand texture, the highest content of mucilage resulted in $D_s(\psi_{soil})$ being around 3.5 times higher than that of the control soil ($D_s(\psi_{soil})$= 7.1×10^{-4} vs 2×10^{-4}).

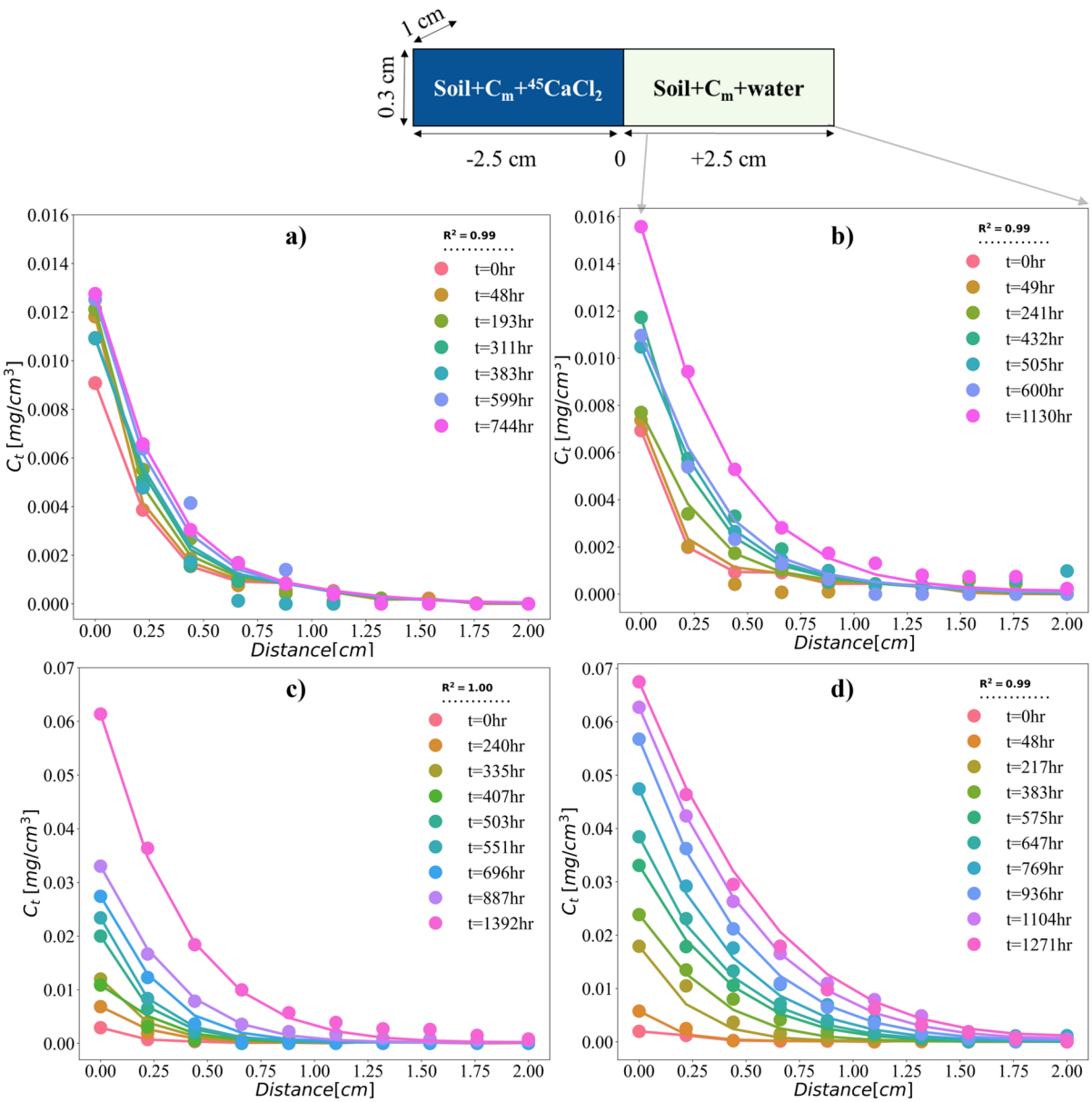

Fig. 3 Example profiles of Ca concentration in the unlabelled compartment at different times (hr) in the loam soils at soil water content (θ_v) of 0.125 [cm^3/cm^3] and treated with varying mucilage contents (C_m) of a) 0.0, b) 2.5, c) 5.0, and d) 7.5 [mg/g]. The dots refer to the measured data of one replication, and the lines are the fitted concentration profiles according to Eq. (1). Distance refers to the length of the unlabelled compartment, positioned 0.5 cm away from the border between the two compartments. Here, only data from unlabelled compartments are used to avoid any potential discontinuities at the interface between the labelled and unlabelled compartments. Note that time zero refers to the data of the first image taken at 2–5 h after diffusion had started. Experiments for the different mucilage treatments were run in separate batches, so scanning intervals are not identical across treatments

In finer soil textures (sandy loam and loam), the reductive effect of mucilage on D_s under wet ranges was less pronounced than in sand (Fig. 5). In loam, the presence of mucilage did not cause a clear reduction in D_s across either the wet or dry range (Fig. 5c). In contrast, in sandy loam, a marked

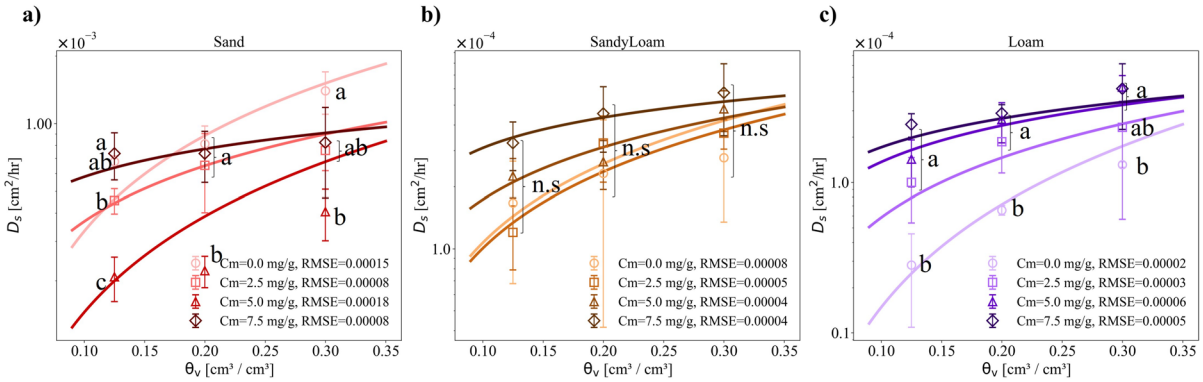

Fig. 4 Mean comparison of measured soil effective diffusion coefficient (D_s), derived from Eq. (1), and the fitted D_s derived from Eq. (5), in mucilage-treated and untreated **a**) sand, **b**) sandy loam, and **c**) loam textures at each selected soil water content (θ_v) of 0.30, 0.20, and 0.125 [cm^3/cm^3]. Data are the average of 4 replications, and the error bars indicate the standard deviation. Different letters indicate significant differences ($\alpha < 0.05$); The lines represent the fitted value and RMSE denotes the root mean square error

Table 3 The soil partition coefficient and fitted parameters presented in Eqs. (5, 7, 8, and 10)

Soil texture	Model Parameters						$C_m\left[\frac{mg}{g}\right]$			
	$D_s(\theta_s)$	β	a	b	c	d	0	2.5	5.0	7.5
	$\left[\frac{cm^2}{hr}\right]$	[-]	[-]	[-]	$\left[\frac{g}{mg}\right]$	$\left[\frac{g^2}{mg^2}\right]$	$K_d\left[\frac{cm^3_{soil\ liquid}}{g\ soil}\right]$			
Sand	0.0023	0.0505	0.1662	1.0586	−1.0206	0.2149	0.3071	0.4149	0.3448	0.5524
Sandy loam	0.0007	0.0100	0.2987	0.8076	0.4446	−0.1269	0.4197	0.3897	0.2909	0.3649
Loam	0.0006	0.0100	0.3574	1.7482	0.4436	−0.0098	0.4295	0.3418	0.3843	0.4830

$D_s(\theta_s)$ effective diffusion coefficient at soil water saturated condition, β viscosity scaling factor, *a, b, c, d* fitting parameters, mucilage content, and partition coefficient

reduction was observed at the lowest mucilage content (C_m = 2.5 mg/g) across all matric potentials, and at the intermediate mucilage content (C_m = 5.0 mg/g) under wet conditions ($\psi_{soil} > -154$ cm) (Fig. 5b). As the soil dried further, ($\psi_{soil} < -154$ cm), mucilage increased D_s, relative to the control, with the magnitude of this enhancement rising with mucilage content (Fig. 5b). At $\psi_{soil} = -1000$ cm, representing the dry range in sandy loam and loam textures, the highest mucilage content (C_m = 7.5 mg/g) increased $D_s(\psi_{soil})$ by approximately 3.6-fold in loam (3.5×10^{-4} vs 9.8×10^{-5}), and 2.2-fold in sandy loam (4×10^{-4} vs 1.8×10^{-4}) compared with their respective control soils. In addition, our findings indicated that the presence of mucilage noticeably attenuated the sharp decline of the $D_s(\psi_{soil})$ during the transition from wet to dry conditions, as reflected by the reduced steepness of the predicted D_s across the shown range of ψ_{soil} in all soil textures (Fig. 5).

Discussion

We showed that soil drying slowed down soil nutrient diffusion, attributed to a reduced cross-sectional area of the liquid phase (connected liquid pathways) and an increased tortuosity of the diffusion pathway. Mucilage helped to counteract these effects by altering the liquid phase redistribution within the pore

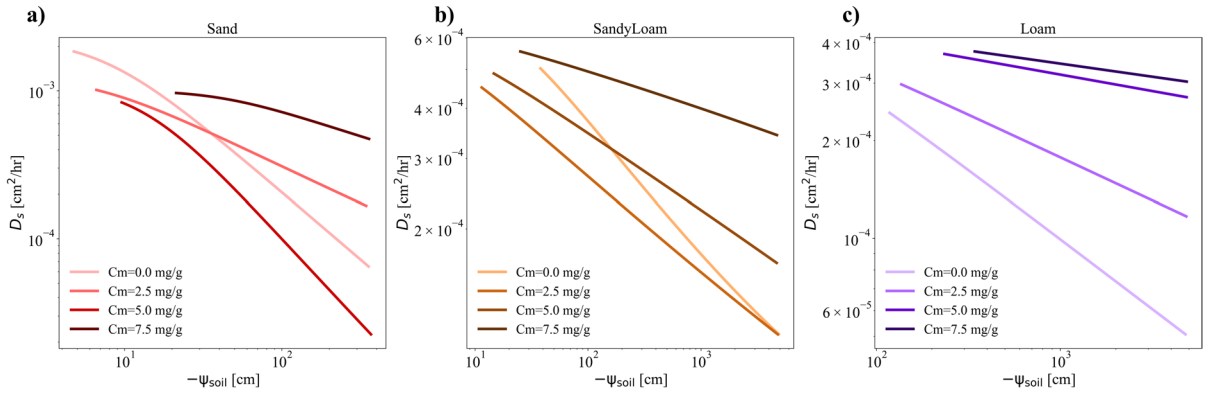

Fig. 5 The predicted soil effective diffusion coefficient (D_s) as a function of soil matric potential (ψ_{soil}) in mucilage-treated and untreated **a**) sand, **b**) sandy loam, and **c**) loam textures versus ψ_{soil} according to Eq. [5]

space, improving water retention, and enhancing liquid connectivity. However, the effectiveness of mucilage was dependent on both its content and soil texture, as a result of different interactions with the soil matrix at the soil pore scales (Kroener et al. 2018; Benard et al. 2021). In finer-textured soils, even lower mucilage contents were sufficient to enhance water retention and diffusion, while in coarser-textured soils, higher mucilage content was required to achieve similar benefits.

Mucilage-mediated water retention and redistribution: soil texture dependence

A key finding of our study is the texture-dependent effectiveness of mucilage in enhancing soil water retention (Fig. 1). To better understand this observation, it is essential to examine the mechanisms through which mucilage influences water retention. Mucilage has a multifaceted impact on soil water retention, simultaneously affecting surface tension, capillary retention, and pore structure. It has been shown that mucilage reduces the surface tension of the liquid phase (Naveed et al. 2019), which weakens capillary forces and promotes earlier pore drainage (Read and Gregory 1997; Naveed et al. 2019; Benard et al. 2021). However, mucilage's intrinsic water-holding capacity and ability to modify soil pore structure counteract this effect by stabilizing water films and enhancing retention. These processes occur concurrently, with their relative magnitudes determining the net impact of mucilage on water retention. While mucilage's influence on surface tension and water retention is strongly content-dependent, our study demonstrated that its emerging overall effect is highly texture-dependent (Figs. 1a, b, and c). Loamy soil exhibited a significantly stronger response to mucilage compared to sand and sandy loam soils, showing higher water content across all tested contents, particularly in the dry range (ψ_{soil}= –23,608 cm). This suggests that in finer-textured soils, mucilage integrates more effectively with the soil matrix and the pore network, leading to greater water retention at lower mucilage content (Fig. 1f).

In contrast, sandy soil required a higher mucilage content before any significant increase in water retention was observed (Fig. 1a). Water retention in sandy soil remained statistically unchanged until mucilage reached a critical mucilage content (C_m) of 7.5 mg/g, at which a twofold increase was observed at ψ_{soil}= –37 cm (Fig. 1d). This threshold reflects the challenges posed by the larger pore structure in sandy soils, where mucilage must reach sufficiently high contents to form a continuous, spanning network across large pores. Unlike loam, where mucilage can readily bridge smaller pores even at low contents, sandy soils require a higher mucilage content to achieve a similar effect (Kroener et al. 2018; Benard et al. 2019).

The observed increase in water retention in loamy soil cannot be solely attributed to the intrinsic water-holding capacity of pure mucilage, as similar effects were not observed in sandy soil or other textures where mucilage was present. Instead, we propose that the key factor lies in the interaction between mucilage

and the soil matrix at the pore scale. Loamy soil has a higher surface area and more active charge sites, which promote stronger molecular interactions between mucilage and soil particles (Benard et al. 2019). This allows mucilage to absorb onto soil surfaces and form a stable, interconnected network within the pore structure. Once mucilage forms such a network, it acts as an additional adsorptive retention mechanism, effectively enhancing soil water retention beyond its intrinsic gel-water capacity (Benard et al. 2021; Williams et al. 2021; Esmaeelipoor Jahromi et al. 2022). Beyond adsorption, mucilage bridging across the pore space can modify the pore size distribution, shifting the overall soil pore structure toward a narrower range with stronger capillary retention. By stabilizing water within these smaller, well-connected pores, mucilage prevents rapid drainage, ensuring that moisture remains available for longer periods. Additionally, loamy soil has smaller pores, which, together with the high viscosity of mucilage, induces greater frictional resistance on the liquid phase during drainage. This frictional effect delays the recession of the liquid phase at the pore scale during soil drying, further enhancing water retention and redistribution within the pore network (Benard et al. 2021). The limited impact of mucilage in sandy loam was an unexpected finding, particularly given that at$\left(C_m\right)$ of 7.5 mg/g, a significant increase in water retention was observed in sandy soil, whereas in sandy loam, the effect remained statistically insignificant despite moving to a finer soil texture (Fig. 1e). A key factor explaining this behaviour is the inherently higher capillary retention capacity of sandy loam compared to sandy soil. Unlike sandy soil, where large pores induce weak capillary retention, sandy loam already contains a more structured pore network that can hold water efficiently even without mucilage. In this texture, mucilage's ability to enhance capillary-driven retention may be less pronounced, as the soil's natural pore structure already generates strong capillary forces. Our results further indicate that mucilage's influence on sandy loam was particularly negative at near-saturation conditions, where we observed a reduction in water retention (Fig. 1b). This is likely due to mucilage's ability to lower surface tension, which promotes earlier pore drainage (Carminati et al. 2017; Naveed et al. 2019). However, as soil dries, mucilage content in the liquid phase increases, shifting its role from modifying surface tension to stabilizing water within pores. This transition resulted in a 1.2-fold increase in water content at the dry range compared to the control in the presence of mucilage at $\left(C_m\right)$ of 7.5 mg/g, but this increase was not yet statistically significant (Fig. 1e). When moving to finer soil textures, this increase in retention was further reinforced through stronger interactions with soil pore walls, ultimately leading to a significant increase in water retention (Fig. 1f).

Mucilage effect on soil effective diffusion

Our results demonstrate that the effect of mucilage on D_s depends on soil texture, mucilage content (C_m), and whether D_s is evaluated as a function of soil water content or soil matric potential. The overall effect of mucilage can be attributed to three key processes: (i) increasing viscosity of liquid phase and therefore reducing D_s, (ii) enhancing liquid-phase connectivity and therefore maintaining a higher D_s, and (iii) increasing water holding capacity of soils and therefore maintaining a higher D_s at a given soil matric potential (ψ_{soil}). In sandy soil at higher moisture levels (near saturation), the dominant effect of mucilage is viscosity-induced diffusion resistance, which reduces $D_s(\theta_v)$ by restricting molecular movement (D_0). This observation aligns with the observation of Chenu and Roberson (1996) who reported a reduced diffusivity of glucose by EPS (Chenu and Roberson 1996). In sandy loam and loam soils, however, the viscosity-induced reduction was not observed at any mucilage content under the examined soil water contents (Fig. 4b and c). A key question here is why the viscosity-induced reduction in D_s was not observed in sandy loam and loam soils. This discrepancy can be explained by differences in mucilage interactions with soil particles. When mucilage is assumed to be fully dissolved in free water, without interaction with the surrounding medium, its concentration increases exponentially as water content decreases. This leads to a substantial rise in viscosity according to Eq. (7), and consequently, a significant reduction in D_s, as described by Eq. (5). However, this behaviour does not hold when mucilage is embedded within a porous medium such as soil. In such environments, mucilage viscosity-driven effect is strongly modulated by soil texture, indicating that the effectiveness of mucilage in altering system viscosity is closely tied to the physical characteristics of the soil matrix.

In finer-textured soils (sandy loam and loam), which contain higher clay and silt fractions with more active surface charges, mucilage is more likely to bind to soil particle surfaces rather than remaining freely present in the bulk liquid phase at high contents, where it would otherwise increase viscosity. As a result, its impact on D_s via viscosity changes is diminished. Moreover, in finer-textured soils, the smaller pore geometry facilitates faster and more extensive spreading of mucilage, promoting the rapid formation of a continuous gel network. This increases the likelihood of phase separation compared to coarser soils, where the larger pores delay or limit network formation. As a result, once the gel phase is established, the amount of free mucilage in the liquid phase decreases, thereby reducing its contribution to viscosity enhancement. Another possible explanation for the lack of a viscosity-induced reduction in D_s in sandy loam and loam soils is that mucilage plays a stronger role in improving liquid-phase connectivity in fine-textured soils compared to coarse-textured soils. In these finer soils, the enhancement of water-filled pathway connectivity may outweigh the negative effect of increased viscosity, leading to an overall improvement in D_s despite mucilage's thickening properties.

The second mechanism by which mucilage impacts D_s at the same θ_v is by influencing water redistribution within the pore space, ultimately maintaining its connectivity during soil drying (Benard et al. 2019; Zarebanadkouki et al. 2019). In contrast to the behaviour observed in sandy soils, mucilage treatment improved D_s in sandy loam and loam (Fig. 4b and c), demonstrating a strong positive correlation between mucilage content and D_s in both soil types. This effect was particularly significant in loam, even at lower θ_v, as shown in Fig. 4c. The enhanced D_s, particularly in loam, as the finest soil texture can be attributed to improved connectivity of water-filled pathways. The underlying mechanisms, discussed in detail in the previous section, suggest that increased interaction between mucilage and soil particles leads to the formation of thicker and more stable water films and capillary bridges within the pore spaces. This stabilized liquid phase helps maintain hydraulic continuity, facilitating the diffusive transport of nutrients.

The third mode of mucilage's impact on D_s is through its effect on soil water-holding capacity. Mucilage-treated soils retain more water than untreated bulk soil at the same ψ_{soil}, leading to higher moisture levels in the rhizosphere (Fig. 1). To fully assess mucilage's effect on diffusion, it is essential to evaluate D_s as a function of ψ_{soil}, as this approach captures the overall impact of mucilage on D_s, including its effects on altered liquid viscosity, enhanced liquid-phase connectivity, and increased water retention. This assessment allows for a direct comparison of D_s in bulk soil (control soil) with the emerging D_s in the rhizosphere, where mucilage is present at varying C_m across different soil textures. Our results (Fig. 5) demonstrated that the impact of mucilage on D_s was the strongest whenever mucilage significantly increased the soil's water-holding capacity. This trend was particularly evident at high C_m across all tested soil textures, where mucilage prevented a rapid decline in D_s under drying conditions. In finer soil textures, as illustrated in Fig. 5b and c, the beneficial effect of mucilage was more pronounced, largely due to the less dominant effect of mucilage on liquid-phase viscosity compared to sandy soil (previously explained). Given these observations, in sandy loam, the increase in $D_s(\psi_{soil})$ can be predominately attributed to the impact of mucilage on water redistribution and enhancement of liquid connectivity as no significant impact on water content was observed (Fig. 1e). In loam soil; however, the influence of mucilage on both water-holding capacity (Fig. 1c and f) and water redistribution (Fig. 4c), resulting in a wetter and more interconnected liquid phase. This, in turn, led to higher $D_s(\psi_{soil})$, the magnitude of which was dependent on mucilage content.

To further elaborate on the effect of mucilage on the D_s and its emergent impact on soil–plant nutrient relations, let us consider a scenario involving a single root growing in loam soil under a matric potential of $\psi_{soil} = -5000$ cm, representing a moderate dry condition. For simplicity, we will assume a night-time scenario where transpiration is negligible, allowing the soil water potential to approach equilibrium between the rhizosphere and the bulk soil. Under this ψ_{soil}, our findings indicated that the $D_s(\psi_{soil})$ of rhizosphere soil treated with C_m of 2.5, 5.0, and 7.5 mg/g was approximately 2.4-, 5.4-, and sixfold greater in comparison with untreated bulk soil, respectively (Fig. 5c). This improvement underscores the crucial role of mucilage in mitigating the adverse effects of soil drying on D_s. Consistent with our findings, a modelling study by Zarebanadkouki et al. (2019) demonstrated that an increase in D_s delayed nutrient deficiency by slowing the development of depletion zones around roots,

particularly for nutrients in low contents in the liquid phase. Higher D_s facilitates more effective diffusion toward the root, preventing severe nutrient gradients from forming. This enhancement became particularly relevant under dry conditions, where the movement of nutrients is primarily diffusion-limited (Olsen et al. 1962; Kuchenbuch et al. 1986; Bhadoria et al. 1991). Zarebanadkouki et al. (2019) also highlighted that mucilage helps mitigate salinity stress by improving the diffusive flux of solutes away from the root surface. In saline soils, where high concentrations of salts tend to accumulate at the root-soil interface due to mass flow-driven transport, enhanced D_s resulting from mucilage presence can delay harmful salt build-up by promoting the back-diffusion of solutes during periods of reduced transpiration, like during night-time.

While our experimental approach provided valuable insights into mucilage-mediated Ca diffusion, several limitations should be acknowledged. First, we used ^{45}Ca as a tracer to track solute movement; however, Ca^{2+} ions can also interact with acidic polysaccharide groups in mucilage, forming ionic cross-links that may alter the structural and rheological properties of the mucilage network. Such interactions could potentially increase mucilage microstructural stability or modify its hydration dynamics compared to the freshly extracted state (Brax et al. 2020). Although we cannot fully exclude this effect, it is important to note that Ca^{2+} ions are ubiquitous in soil solutions, and their incorporation into the mucilage matrix would naturally occur in situ. Our use of ^{45}Ca therefore likely reflects a realistic, albeit possibly accelerated, scenario of Ca–mucilage interaction in soils. Another factor worth considering is the duration of the diffusion experiment, which spanned several weeks (~9 weeks). Over this period, partial biodegradation of mucilage by residual microbial activity cannot be entirely ruled out. Although soils were pre-treated by ashing at 500–600 °C to remove organic matter and reduce microbial abundance, some recolonization or reactivation could have occurred during the experiment. Such degradation would likely reduce mucilage viscosity and connectivity effects over time.

Conclusion

This study explored the impact of varying contents of plant-derived mucilage on soil water retention and the effective diffusion coefficient across different soil textures. Our findings underscore the pivotal role of soil texture in shaping how plants engineer their rhizosphere to optimize resource utilization under deficit conditions. We found that in coarse-textured soils like sand, larger mucilage content is needed to effectively modify rhizosphere hydraulic properties. In contrast, in finer-textured soils, plants might achieve an improved soil hydraulic and transport properties with a much smaller amount of mucilage.

Author contributions Bahareh Hosseini and Mohsen Zarebanakouki contributed to the conception and design of the study, as well as the collection and analysis of data. Maire Holz and Rainer Remus contributed to the conception and design of the study. Meysam Cheraghi, Daniel Sebastian Moser, and Valerie Pusch were instrumental in collecting data. The initial manuscript draft was composed by Bahareh Hosseini, and all authors provided feedback on preceding drafts. Each author has thoroughly read and given their approval for the final version of the manuscript.

Funding Open Access funding enabled and organized by Projekt DEAL. This research was supported by the Deutsche Forschungsgemeinschaft (DFG) through an individual grant [Grant Number: 459978475]. The author would like to thank the DFG for their financial support.

Data availability The datasets generated during and/or analysed during the current study are available from the corresponding author upon reasonable request.

Declarations

Competing interest The authors have no relevant financial or non-financial interests to disclose.

References

Abdalla M, Carminati A, Cai G, Ahmed MA (2024) Mucilage facilitates root water uptake under edaphic stress:

first evidence at the plant scale. Ann Bot 1–10:mcae193. https://doi.org/10.1093/aob/mcae193
Adamczewski R, Kaestner A, Zarebanadkouki M (2024) Rhizosphere hydraulic regulation in maize: tailoring rhizosphere properties to varying soil textures and moistures. Plant Soil. https://doi.org/10.1007/s11104-024-06840-2
Ahmed MA, Kroener E, Holz M et al (2014) Mucilage exudation facilitates root water uptake in dry soils. Funct Plant Biol 41(11):1129–1137
Barber SA, Walker JM, Vasey EH (1963) Mechanisms for the movement of plant nutrients from the soil and fertilizer to the plant root. J Agric Food Chem 11:204–207. https://doi.org/10.1021/jf60127a017
Benard P, Zarebanadkouki M, Brax M et al (2019) Microhydrological niches in soils: how mucilage and EPS alter the biophysical properties of the rhizosphere and other biological hotspots. Vadose Zone J 18:1–10. https://doi.org/10.2136/vzj2018.12.0211
Benard P, Schepers JR, Crosta M et al (2021) Physics of viscous bridges in soil biological hotspots. Water Resour Res. https://doi.org/10.1029/2021wr030052
Bhadoria PBS, Kaselowsky J, Claassen N, Jungk A (1991) Phosphate diffusion coefficients in soil as affected by bulk density and water content. Z Pflanzenernahr Bodenk 154:53–57. https://doi.org/10.1002/jpln.19911540111
Bienert MD, Werner LM, Wimmer MA, Bienert GP (2021) Root hairs: the villi of plants. Biochem Soc Trans 49:1133–1146
Brax M, Buchmann C, Kenngott K et al (2020) Influence of the physico-chemical properties of root mucilage and model substances on the microstructural stability of sand. Biogeochemistry 147:35–52. https://doi.org/10.1007/s10533-019-00626-w
Carminati A (2013) Rhizosphere wettability decreases with root age: a problem or a strategy to increase water uptake of young roots? Front Plant Sci 4:298
Carminati A, Moradi AB, Vetterlein D et al (2010) Dynamics of soil water content in the rhizosphere. Plant Soil 332:163–176. https://doi.org/10.1007/s11104-010-0283-8
Carminati A, Benard P, Ahmed MA (2017) Liquid bridges at the root-soil interface. Plant Soil. https://doi.org/10.1007/s11104-017-3227-8
Chenu C, Roberson EB (1996) Diffusion of glucose in microbial extracellular polysaccharide as affected by water potential. Soil Biol Biochem 28:877–884. https://doi.org/10.1016/0038-0717(96)00070-3
Chou H, Wu L, Zeng L, Chang A (2012) Evaluation of solute diffusion tortuosity factor models for variously saturated soils. Water Resour Res 48:1–11. https://doi.org/10.1029/2011WR011653
Esmaeelipoor Jahromi O, Knott M, Mysore Janakiram RK et al (2022) Pore-scale simulation of mucilage drainage. Vadose Zone J. https://doi.org/10.1002/vzj2.20218
Ghanbarian B, Daigle H, Hunt AG et al (2015) Gas and solute diffusion in partially saturated porous media: percolation theory and effective medium approximation compared with lattice Boltzmann simulations. Journal of Geophysical Research: Solid Earth 120:182–190. https://doi.org/10.1002/2014JB011645
Hayat F, Abdalla M, Munir MU (2021) Effect of chia seed mucilage on the rhizosphere hydraulic characteristics. Sustainability. https://doi.org/10.3390/su13063303
Holz M, Zare (Zarebanadkouki) M, Benard P et al (2024b) Root and rhizosphere traits for enhanced water and nutrients uptake efficiency in dynamic environments. Front Plant Sci 15:1383373. https://doi.org/10.3389/fpls.2024.1383373
Holz M, Zarebanadkouki M, Carminati A, Kuzyakov Y (2019) Visualization and quantification of root exudation using ^{14}C imaging: challenges and uncertainties. Plant Soil 437:473–485. https://doi.org/10.1007/s11104-019-03956-8
Holz M, Mundschenk E, Pusch V et al (2024a) Visualizing and quantifying 33P uptake and translocation by maize plants grown in soil. Front Plant Sci 15:1–11. https://doi.org/10.3389/fpls.2024.1376613
Hosseini B, Cheraghi M, Hiesch S et al (2024) Contrasting rhizosheath formation capacities in two maize inbred lines: implications for water and nutrient uptake. Plant Soil. https://doi.org/10.1007/s11104-024-06883-5
James G, Witten D, Hastie T et al (2023) An introduction to statistical learning: With applications in python. Springer Nature. https://doi.org/10.1007/978-3-031-38747-0
Kroener E, Holz M, Zarebanadkouki M et al (2018) Effects of mucilage on rhizosphere hydraulic functions depend on soil particle size. Vadose Zone J 17(1):170056. https://doi.org/10.2136/vzj2017.03.0056
Kuchenbuch R, Claassen N, Jungk A (1986) Potassium availability in relation to soil moisture - I. Effect of soil moisture on potassium diffusion, root growth and potassium uptake of onion plants. Plant Soil 95:221–231. https://doi.org/10.1007/BF02375074
Lynch JP (2013) Steep, cheap and deep: an ideotype to optimize water and N acquisition by maize root systems. Ann Bot 112:347–357
McCully ME, Boyer JS (1997) The expansion of maize root-cap mucilage during hydration. 3. Changes in water potential and water content. Physiol Plant 99:169–177. https://doi.org/10.1111/j.1399-3054.1997.tb03445.x
Moldrup P, Olesen T, Komatsu T et al (2001) Tortuosity, diffusivity, and permeability in the soil liquid and gaseous phases. Soil Sci Soc Am J 65:613–623. https://doi.org/10.2136/sssaj2001.653613x
Moradi AB, Carminati A, Vetterlein D et al (2011) Three-dimensional visualization and quantification of water content in the rhizosphere. New Phytol 192:653–663. https://doi.org/10.1111/j.1469-8137.2011.03826.x
Moradi AB, Carminati A, Lamparter A et al (2012) Is the rhizosphere temporarily water repellent? Vadose Zone J 11:vzj2011.0120. https://doi.org/10.2136/vzj2011.0120
Naveed M, Brown LK, Raffan AC et al (2017) Plant exudates may stabilize or weaken soil depending on species, origin and time. Eur J Soil Sci 68(6):806–816. https://doi.org/10.1111/ejss.12487
Naveed M, Ahmed MA, Benard P et al (2019) Surface tension, rheology and hydrophobicity of rhizodeposits and seed mucilage influence soil water retention and hysteresis. Plant Soil 437:65–81. https://doi.org/10.1007/s11104-019-03939-9

Newville M, Otten R, Nelson A, et al (2021) lmfit/lmfit-py: 1.0. 3. Zenodo

Olsen SR, Kemper WD, Jackson RD (1962) Phosphate diffusion to plant roots. Soil Sci Soc Am J 26:222–227

Ortas I, Ustuner O (2014) The effects of single species, dual species and indigenous mycorrhiza inoculation on citrus growth and nutrient uptake. Eur J Soil Biol 63:64–69. https://doi.org/10.1016/j.ejsobi.2014.05.007

Philippot L, Raaijmakers JM, Lemanceau P, Van Der Putten WH (2013) Going back to the roots: the microbial ecology of the rhizosphere. Nat Rev Microbiol 11:789–799. https://doi.org/10.1038/nrmicro3109

Phillies GDJ (2007) Optical probe diffusion in polymer solutions. arXiv Prepr arXiv07053222

Raynaud X, Leadley PW (2004) Soil characteristics play a key role in modeling nutrient competition in plant communities. Ecology 85:2200–2214. https://doi.org/10.1890/03-0817

Read DB, Gregory PJ (1997) Surface tension and viscosity of axenic maize and lupin root mucilages. New Phytol 137:623–628. https://doi.org/10.1046/j.1469-8137.1997.00859.x

Rongsawat T, Peltier JB, Boyer JC et al (2021) Looking for root hairs to overcome poor soils. Trends Plant Sci 26:83–94. https://doi.org/10.1016/j.tplants.2020.09.001

Seabold S, Perktold J (2010) Statsmodels: Econometric and Statistical Modeling with Python. Proc 9th Python Sci Conf 92–96. https://doi.org/10.25080/majora-92bf1922-011

Seiffert S, Kaselowsky J, Jungk A, Claassen N (1995) Observed and calculated potassium uptake by maize as affected by soil water content and bulk density. Agron J 87:1070–1077

Van Genuchten MT (1980) A closed-form equation for predicting the hydraulic conductivity of unsaturated soils. Soil Sci Soc Am J 44(5):892–898. https://doi.org/10.2136/sssaj1980.03615995004400050002x

Virtanen P, Gommers R, Oliphant TE et al (2020) Scipy 1.0: fundamental algorithms for scientific computing in Python. Nat Methods 17:261–272

Williams KA, Ruiz SA, Petroselli C et al (2021) Physical characterisation of chia mucilage polymeric gel and its implications on rhizosphere science - Integrating imaging, MRI, and modelling to gain insights into plant and microbial amended soils. Soil Biol Biochem 162:108404. https://doi.org/10.1016/j.soilbio.2021.108404

Zarebanadkouki M, Ahmed MA, Carminati A (2016) Hydraulic conductivity of the root-soil interface of lupin in sandy soil after drying and rewetting. Plant Soil 398:267–280. https://doi.org/10.1007/s11104-015-2668-1

Zarebanadkouki M, Fink T, Benard P, Banfield CC (2019) Mucilage facilitates nutrient diffusion in the drying rhizosphere. Vadose Zone J 18:1–13. https://doi.org/10.2136/vzj2019.02.0021

Zickenrott I, Woche SK, Bachmann J et al (2016) An efficient method for the collection of root mucilage from different plant species—a case study on the effect of mucilage on soil water repellency. J Plant Nutr Soil Sci 179:294–302